ELSEVIER

Journal of Power Sources 67 (1997) 49–59

JOURNAL OF POWER SOURCES

Investigation of thermal phenomena in VRLA/AGM stationary lead/acid batteries with a thermal video imaging system

Herbert Giess *

Accumulatoren-Fabrik Oerlikon, Binzmühlestrasse 94, 8050 Zürich, Switzerland

Received 31 July 1996; accepted 15 August 1996

Abstract

An infrared thermal video imaging system (Model TVS2000) has been used to follow the evolution of heat in VRLA/AGM cells and monoblocs. The system has the capability of resolving 0.05 °C temperature differences within such cells. Minute thermal inhomogeneities are easily detectable and allow the dynamics of the heat evolution to be followed during discharge and charge processes. In large 1000 Ah VRLA/AGM cells, electrolyte movements are traceable with this method through the associated shifting of the site of the oxygen recombination reaction and the subsequent local evolution of heat. The areas of heat evolution match those with the most significant degree of local grid growth. © 1997 Elsevier Science S.A.

Keywords: Thermal imaging; Valve-regulated lead/acid batteries; Heat evolution; Absorptive glass mat; Electrolyte mobility; Lead/acid batteries

1. Introduction

Valve-regulated lead/acid (VRLA) batteries are the systems of choice for the power back-up of multi-media communication highways. In this type of battery, an oxygen-recombination cycle is operative and decreases the amount of electrolyte water that is lost during float charge operation to approximately 1 to 3% of the theoretical value of 0.336 g per Ah. This reduces the need for ventilation and dispenses with regular electrolyte topping-up operations.

For efficient oxygen recombination, a fast mass transport of oxygen from the positive (lead dioxide) plate to the negative (lead sponge) plate of the lead/acid battery is necessary. A rapid transfer is essential in order to avoid a build-up in cell pressure to a level where venting of oxygen through the valve can occur. Fast transport is achievable only through a gas-phase transport by which oxygen can diffuse rapidly throughout open porosity in the glass mat electrolyte absorber.

In order to achieve open porosity in the absorber, a VRLA/AGM (absorptive glass mat) cell is filled with less electrolyte volume than that available from the combined glass mat, negative and positive plate pore volumes. A cell construction condition of 'starved-in-electrolyte' is hence sought for VRLA/AGM cells. The electrolyte is essentially immobilized by surface tension forces at the glass micro-fibres and its macro-mobility is greatly reduced. Thus, the electrolyte in a VRLA cell loses its auxiliary function as a heat-exchange fluid, both within the plate stack itself and between the plate stack and the cell walls.

2. Heat evolution

In lead/acid batteries, the charge and discharge processes and, in VRLA types, also the oxygen-recombination cycle, produce heat within the cell. At extremely low discharge rates, a lead/acid battery displays a heat pump, i.e. cooling effect. The main thermal sources are Joule heating and reaction heat, namely

$$\text{Joule heating (W s or J)}\ Q = I\Delta V\Delta t \quad (1)$$

where I is the float current in A, ΔV the cell voltage-open circuit voltage, and Δt, the time elapsed.

$$\text{Heat of reaction (W s)}\ Q = T\Delta S \quad (2)$$

where T is in °K and ΔS the reaction entropy.

In a lead/acid battery, at a constant float voltage of 2.25 V/cell and without gas recombination, the cells are supplied with energy at the rate of 2.25 V × I (A) and the escaping electrolysis gasses carry 1.48 V × I (A) energy

* Corresponding author. Tel.: +41 (1) 318 84 84; Fax: +41 (1) 318 86 40.

PII S0378-7753(96)02641-9

from the cell [1]. In this way, only about 34% of the float charge energy remains in the cell to generate heat. Due to oxygen recombination, VRLA cells have higher specific float currents (mA/Ah) than flooded systems. Essentially no gas escapes and, thus, all the charging energy is retained in the cell and is converted into heat. VRLA batteries are therefore pushed towards higher operating temperatures and this necessitates careful attention in terms of thermal management.

To gain insight into the level and the spatial distribution of the temperature and to devise strategies for heat dissipation through radiation, convection and conduction, VRLA/AGM cells and monoblocs have been observed in this study under different operating conditions with a thermal video imaging system.

3. Thermal video imaging system

Infrared (IR) radiation has a wavelength of 0.8 to 1000 μm that lies between visible light and microwave radiation. The radiation emitted from a body displays a specific relationship to the intensity and the temperature. In the case of black-body radiation, the relationship is given by

$$W = \sigma T\,(^{\circ}\mathrm{K}) \tag{3}$$

where W is the IR radiant energy (W cm^{-2}), T the absolute temperature in °K, and σ the Stefan–Boltzmann constant.

The higher the temperature on the surface of an object, the more the IR radiation emitted. The intensity of this radiation is dependent on the properties of the emitting body such as material composition and surface condition. Thus, bodies at the same surface temperature do not emit the same amount of IR radiation, i.e. do not have the same emissivity, ϵ. The latter is defined as

$$\epsilon = 1 - (\tau + \Gamma) \tag{4}$$

where ϵ is the emissivity, τ the transmissivity, and Γ the reflectivity. The value ϵ is, for example, 0.09 for polished aluminium, 0.20–0.45 for oxidized lead, 0.80 for paper, and 0.85–0.91 for plastics.

The relation between radiation and the temperature of an object is expressed by

$$W = \epsilon\sigma T^4 \tag{5}$$

where ϵ is the emissivity, σ the Stefan–Boltzmann constant, and T the absolute temperature (°K).

A thermal video imaging system detects IR energy emitted from the individual points of the object, converts it into temperature values, and displays on a television monitor the temperature distribution as a visible image in which a difference in temperature is represented by differences in brightness or colour. The photon detector of such a system absorbs the IR energy and this affects atomic states and free electrons within the semiconducting detector. Since a given amount of energy is necessary to release free electrons and charges, the detector response will depend on the photon wavelength. Common IR radiation detectors are Si, InAs, InSb, HgCdTe elements that have a spectral response suited to the two major spectral windows of the atmosphere (at 3–5 μm and 8–14 μm) used for IR thermography.

An IR thermal video imaging system consists typically of the following units:

1. silicon window/lens and line scan, rotating mirror optics;
2. a photon semiconductor, e.g. an InSb SPRITE detector that converts the IR radiation into electrical charge and that is typically cooled to −187 °C by expanding argon gas;
3. an electronic signal amplifier and converter, and
4. a thermal image processing and display unit.

4. Experimental

4.1. TVS 2000 thermal video system

For investigations of VRLA/AGM cells and monoblocs, a thermal video imaging system of the type TVS-2000 and thermal image analysis software PicEd (supplied by AVIO Nippon Avionics, Tokyo, Japan) were used. Details of the system are shown in Table 1.

Table 1
Details of the thermal video imaging system

Model	TVS 2000 Nippon Avionics
Field of view	15° (H) × 10° (V)
Frame rate	30 Hz
Number of IR scan lines	100
Detector	Indium antimonide (InSb), 10 element array
Detector wave length	3–5.4 μm (relative sensitivity > 20%)
Number of display pixels	256 (H) × 400 (V)
Temperature measurement range	−40 to +950 °C
Minimum resolvable temperature difference	0.1 °C (0.05 °C with image averaging) at 30 °C
Scale accuracy	±4 °C or ±0.4% of the reading

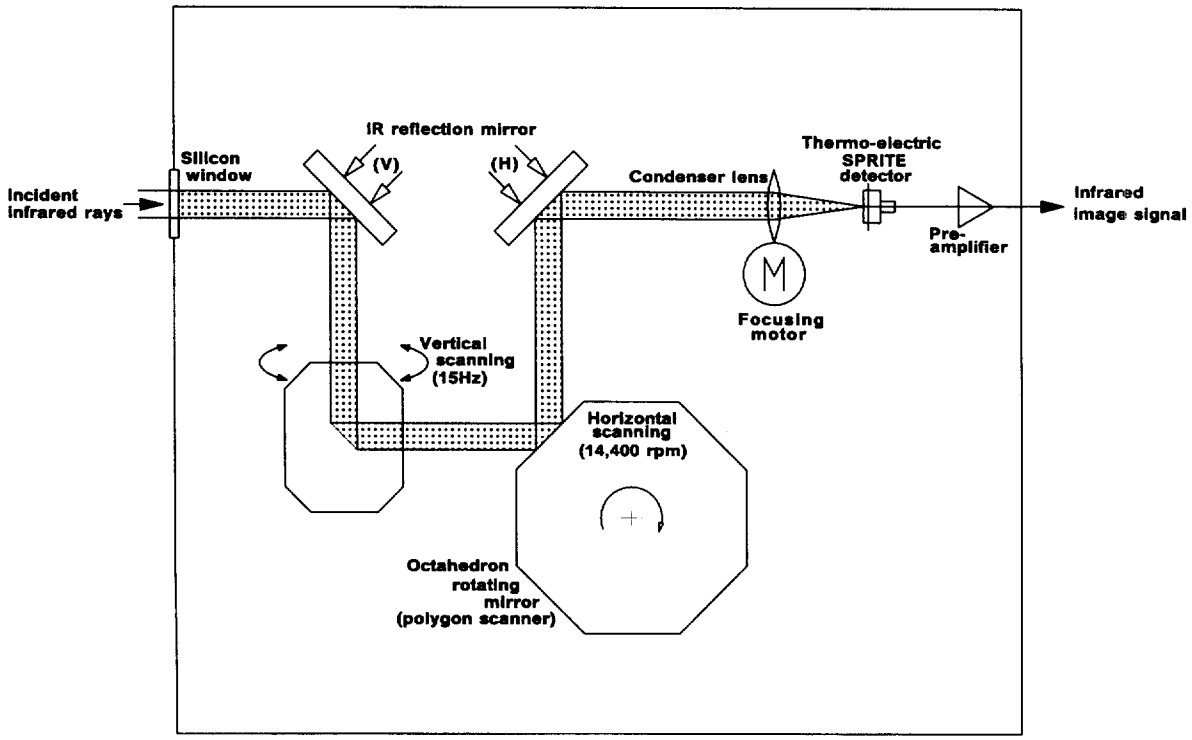

Fig. 1. Positional relationship and shapes of the components of the thermal video imaging 2000 IR camera head.

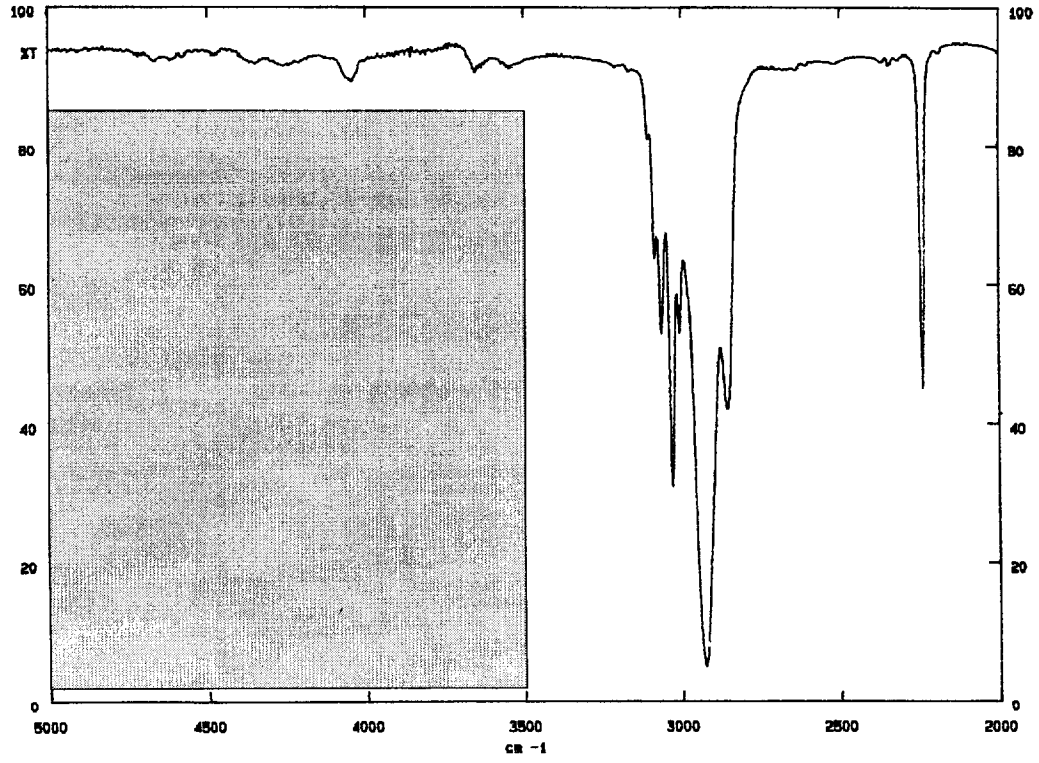

Fig. 2. IR transmittance spectrum of an 8 mm VRLA battery cell wall in ABS. Hatched area indicates InSb detector spectral window.

The positional relationship and shapes of the components of the IR camera head [2] are shown in Fig. 1.

4.2. VRLA cells and monoblocs

The VRLA cells and monoblocs used in the present investigation are of the AGM type and are manufactured by Accumulatoren-Fabrik Oerlikon under the trade name Compact-Power. The units have white acrylonitrile/butadiene/styrene (ABS) plastic cases with a wall thickness that ranges from 5 to 8 mm. The ABS plastic is essentially transparent ($\approx 95\%$ transmission) to IR radiation in the wavelength range 3 to 5.4 μm. The IR transmittance spectrum of the ABS cell case is shown in Fig. 2.

The cells were in the typical starved condition with no free electrolyte in the space between the plate stack and the cell walls. The absence of mobile electrolyte enhances the geometrical definition of the temperature distribution within the cell or monobloc.

4.3. Battery charge and discharge

The discharge and charge of the investigated cells and monoblocs were performed with standard battery testing equipment.

5. Results

5.1. High-rate discharge of a VRLA/AGM monobloc

A 12 V, 26 Ah (C_{10} at 20 °C), VRLA/AGM monobloc was discharged with 73 A (i.e. at 10 min rate) to 1.60 V/cell. The purpose of this test was to determine the evolution of the temperature of the monobloc by looking with the thermal video camera at the long side wall of the monobloc, and to analyse the construction details that cause temperature irregularities. The evolution of the temperature of each cell was followed during discharge, open-circuit stand, and constant-current/constant-voltage charging.

The observed temperature distributions, after 6 and 10 min of discharge, and on open-circuit, after 28 s and 3 min 28 s following the end of discharge, are shown in the Fig. 3. The temperature differential of ~ 1.3 °C between individual cells is vividly displayed in this time sequence with the IR camera directed at the edge of the individual plate stacks. The image shows the pronounced heating of the cell, marked (1), that is noticeable 6 min into the discharge with the monobloc at an average voltage of 1.84 V/cell. Whereas the heating of plate stack (1) occurs with a certain regularity over the entire height of the plate stack,

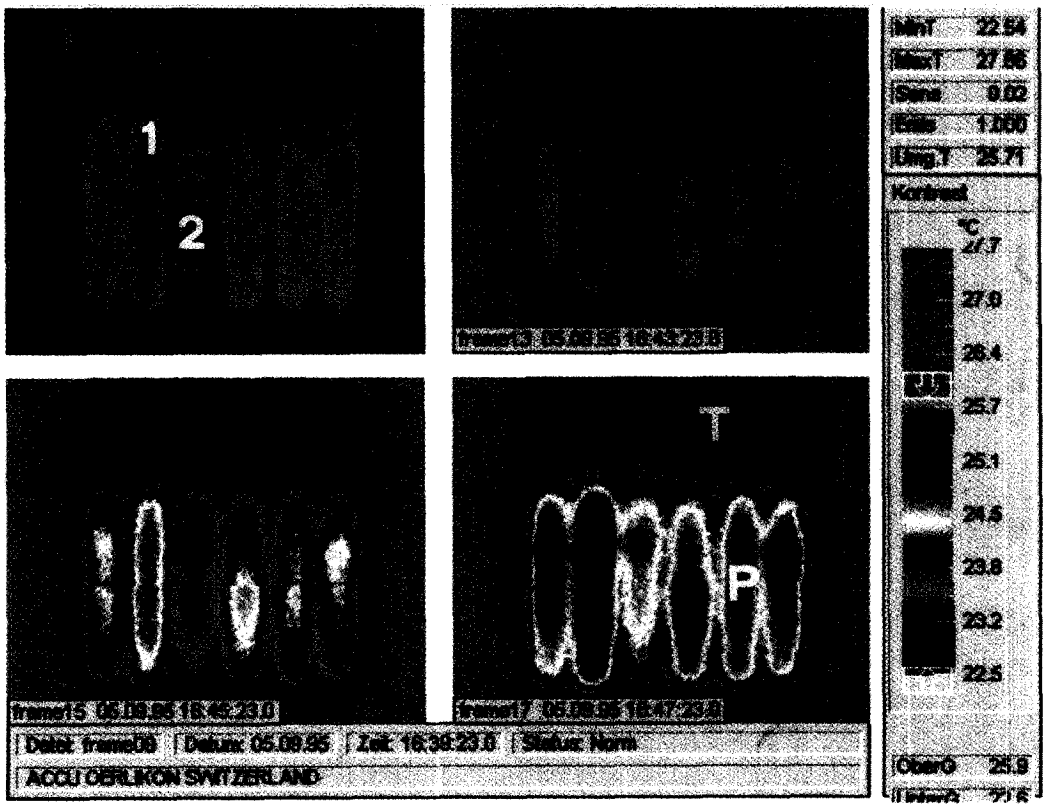

Fig. 3. False colour images edited with the PicEd software showing the long side of a 12 V, 26 Ah VRLA/AGM monobloc and the evolution of the temperature distribution in each cell (temperature range 22.5–25.7 °C). Note the well-defined heat image of the plate stack (P) and the essentially cool cell-head space (T).

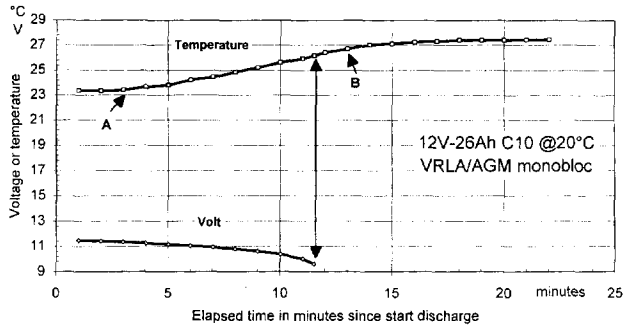

Fig. 4. Evolution of monobloc voltage and maximum IR monobloc temperature during a 73 A (600 s) discharge to 9.6 V (1.60 Vpc).

two other stacks show pronounced hot spots ($\Delta T \approx +0.6$ °C) in both the upper and the lower halves of the stack. One plate stack (2) stays remarkable cooler than the average ($\Delta T \approx -0.4$ °C).

The evolution of the maximum surface temperature in the plate stack volume, as determined from a sequence of images, together with that of the monobloc discharge voltage is shown in Fig. 4. The first rise in temperature can be detected after 3 min of discharge (point A) and is followed by an essentially linear rise until 2 min past the stop of the discharge (point B). The maximum rise of temperature of the observed monobloc wall was ≈ 4 °C.

The differential temperature evolution, as observed with the IR camera, is particularly convenient for the detection of irregular cell polarization behaviour in VRLA cells and monoblocs where access for reference electrodes can be achieved only by destructive means. Any deficient monoblocs or cells thus detected can then be submitted to follow-up analysis. Small differences in plate-stack compression and active-mass formation levels were detected by their influence on local heat generation.

With the PicEd thermal image analysis software, line profiles can be reproducibly placed onto the same position of the thermal image and sequential temperature profiles of the object can be determined. The profile before the start of discharge is shown in Fig. 5. The temperature across the monobloc wall varies between 22.9 and 23.2 °C. Again, a slight temperature differentiation of the cell head space is noticeable.

In Fig. 6, the temperature profile at the end of the 11 min complete discharge to 1.60 V/cell is shown at the exact same location as in Fig. 5. Again, the net separation of the plate stack and the head space in terms of local temperature is clearly discernible. Due to the high sensitivity of the TVS2000 system, achieved by image averaging, the exact location of the plate stack in an AGM/VRLA battery can be easily determined without a heat-generating discharge. Under optimum instrument settings, the 'hot'

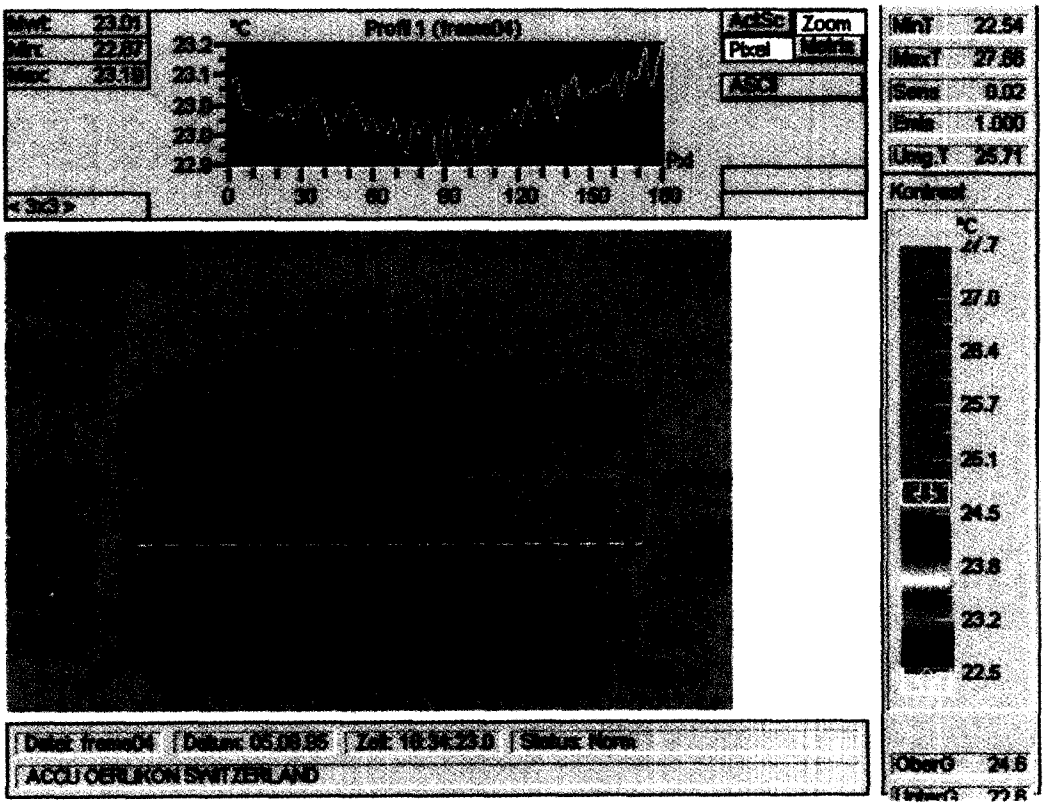

Fig. 5. Line profile of the temperature along the long wall of a 12 V, 26 Ah, VRLA/AGM monobloc at the start of the 73 A discharge. Average temperature at the line profile is 23.01 °C with a minimum of 22.87 °C and a maximum of 23.19 °C.

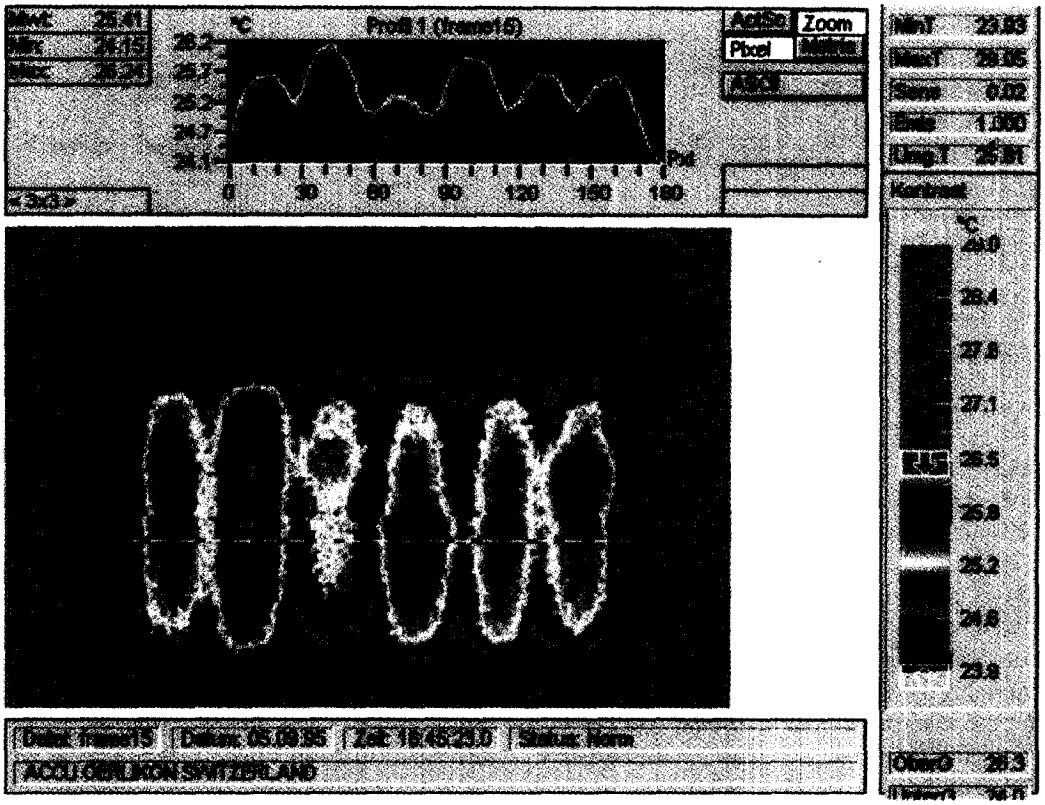

Fig. 6. Line profile of the temperature along the long wall of a 12 V, 26 Ah, VRLA/AGM monobloc at the end of the 73 A discharge. Average temperature at the line profile is 25.41 °C with a minimum of 24.15 °C and a maximum of 26.24 °C.

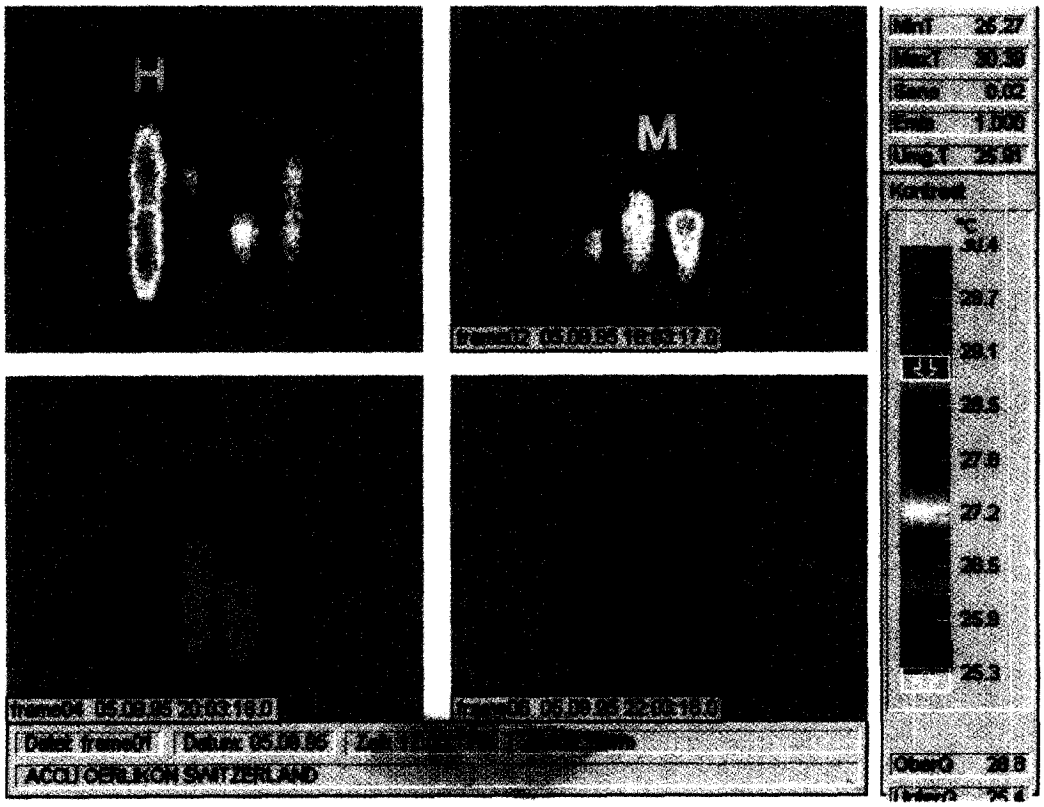

Fig. 7. Sequence of the temperature distribution in a 12 V, 26 Ah, VRLA/AGM monobloc during a constant-current/constant-voltage recharge process. The first, software edited, false-colour image (top left) was taken 18 min after the end-of-discharge or 10 min into the 26 A constant-current charge. The 'hot' cell is still at (H). Remaining images were taken after 1, 2 and 4 h of charge.

air plume that rises from a slightly warmer cell wall is detectable as a flickering in the false-colour display.

After the complete discharge of the 12 V, 26 Ah, VRLA/AGM monobloc, during which 14.01 Ah or 53% of the rated C_{10} capacity was withdrawn, a constant current (CC)–constant voltage (CV) charge was initiated. The charging current was set at 26 A ($10 \times I_{10}$) and the charging voltage was limited to 2.28 V/cell. The evolution of the monobloc temperature distribution was followed with the IR camera and is displayed as a four-image sequence in Fig. 7. The first image, taken after about 10 min of 26 A charge, still shows the temperature distribution as induced by the discharge process. The second image (clockwise) is taken 1 h later with the monobloc now already in the CV (2.28 V/cell) phase of the charging process. At this stage, about 70% of the previously extracted Ah (14 Ah) have been returned. The temperature distribution now shows that the two innermost cells (M) of the monobloc are the site of a higher temperature with the previously 'hot' cell (H) cooled down. This temperature distribution pattern is maintained over the remaining charge as shown in the images 3 and 4 taken, respectively, 2 and 4 h later.

5.2. Orientation-dependent heat evolution sites in large VRLA / AGM cells

Large VRLA/AGM cells with individual capacities that range from 500 to 2000 Ah are generally built with plates for which the height is approximately double the width. In such 'tall' VRLA/AGM cells, there occur small gravity-induced shifts in the electrolyte saturation level in the glass-mat absorber. These shifts create local, enhanced amounts of open porosity, i.e. channels for efficient oxygen-gas transport. The oxygen gas is thus channelled preferentially though this porosity, reacts with the negative sponge lead, and generates heat. This heat, in turn, increases local current flow and enhances the corrosion of the positive grid. It is therefore of interest to detect, through thermal image analysis, the position-dependent differences in temperature under benign and abusive float conditions in such 'tall' VRLA/AGM cells.

For this purpose 2 V, 1000 Ah (C_{10} at 20 °C), VRLA/AGM cells were operated with the plates in: (i) a vertical position (VP) as in traditional flooded cell operation, and (ii) a horizontal position (HPH) with the plates in a 'pan cake' arrangement. Thus, in the IR imaging, the camera looks in position (i) and (ii) at the plate edges and the cell wall, respectively.

The internal details of the 2 V, 1000 Ah, VRL/AGM cell are shown in Fig. 8. The white ABS cell container is replaced by a transparent styrene/acrylonitrile (SAN) cell container. The cell container has the dimensions 210 mm $\times$ 254 mm $\times$ 466 mm ($W \times L \times H$) and contains 20 positive and 21 negative plates. The bottom of the cell is filled with a structural, closed cell foam. Each VRLA cell has two terminals per polarity and an IEC 896-2 rated short-

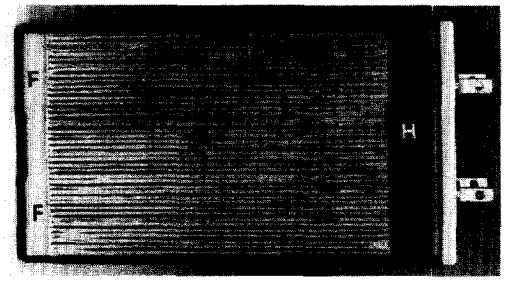

Fig. 8. View of 2 V, 1000 Ah, VRLA/AGM cell in horizontal position with the plates in a 'pan cake' arrangement: (F) bottom foam; (ST) plate stack; (H) head space, and (T) terminals.

circuit current of 18 200 A. In order to assure a homogeneous IR background, each cell was fitted into a tight window cut into a larger sheet of structural plastic foam. The heat dispersion from the cell wall was unimpeded, except for the surface on which the cell rested. The convective (natural) vertical air velocity at the cell walls was ~ 0.05–0.08 m s^{-1}. The two cells were tested in parallel and the temperature distributions were measured at essentially the same moment so that influences of the surrounding environment could be neglected.

5.2.1. Temperature distribution under benign float conditions

The 2 V, 1000 Ah cells were float-charged in parallel at 2.25 V/cell for approximately 1 year before the test. The float current was $\approx$ 77 mA (VP) and $\approx$ 113 mA (HPH) at 20 °C. A separate temperature measurement of the imaged cell wall with a surface probe thermometer gave temperature readings between 19.5 and 20.6 °C.

The temperature distributions of the cells in the above-defined orientations (VP, HPH) were determined at a room (air) temperature of $\approx$ 18–19 °C; the results are shown in Figs. 9 and 10. The false-colour temperature distribution images clearly delineate in the two cells the plate stack (ST) at a temperature of 20.7–20.8 °C and also the bottom foam volume and the head space. The maximum temperature in each orientation is essentially the same, i.e. 20.96–20.98 °C. Within the resolution of the thermal imaging system no major temperature inhomogeneities in the stack were detectable under this operating condition.

5.2.2. Temperature distribution under abusive float conditions

The float voltage of the two test cells was raised in 0.05 V/cell steps and 24 h equilibration periods from 2.25 to 2.50 V/cell. The evolution of the temperature distribution was followed with the IR camera.

The temperature distribution at 2.50 V/cell and a float current of 2750 mA (HPH) and 2150 mA (VP) is shown in Figs. 11 and 12, respectively. The distribution is typical for each operating position. For the vertically positioned cell stack (Fig. 11), the heat evolution takes place in the upper third of the stack. It is in this volume that the combination

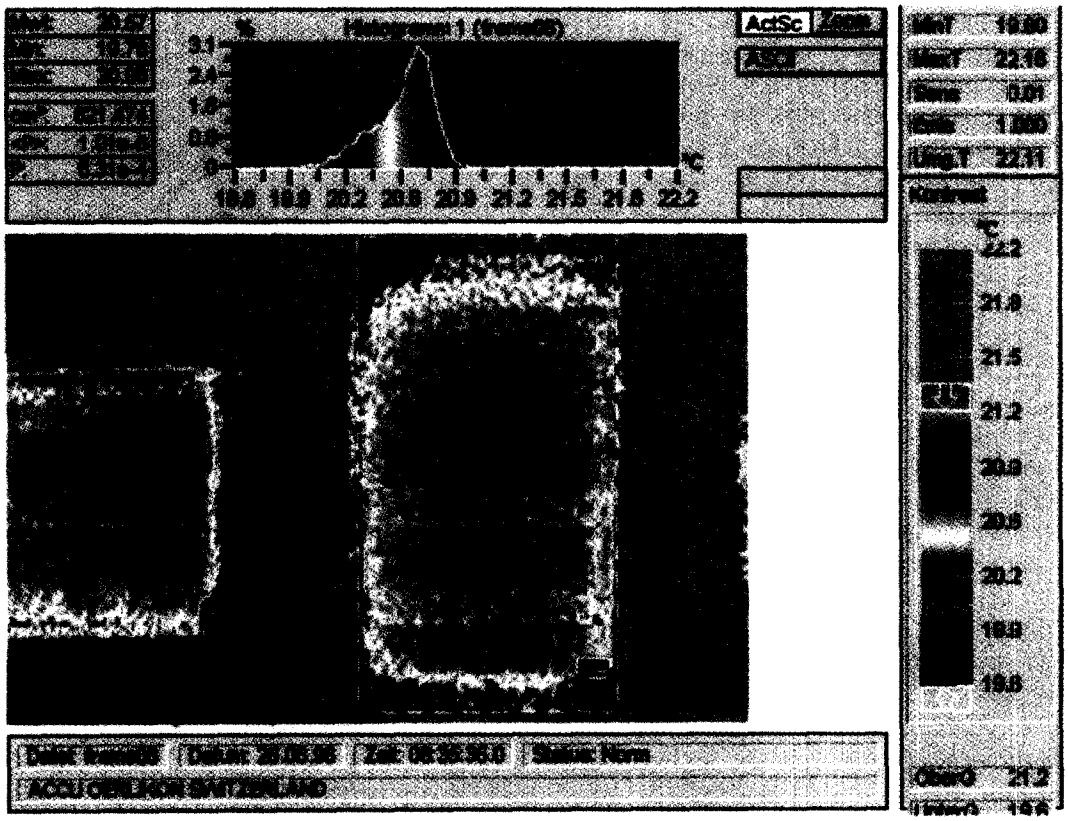

Fig. 9. False-colour temperature distribution image of a 2 V, 1000 Ah, cell in a vertical position (VP) with (H) head space, (ST) plate stack and (F) foam bottom volume. Benign float condition of 2.25 V/cell at room temperature.

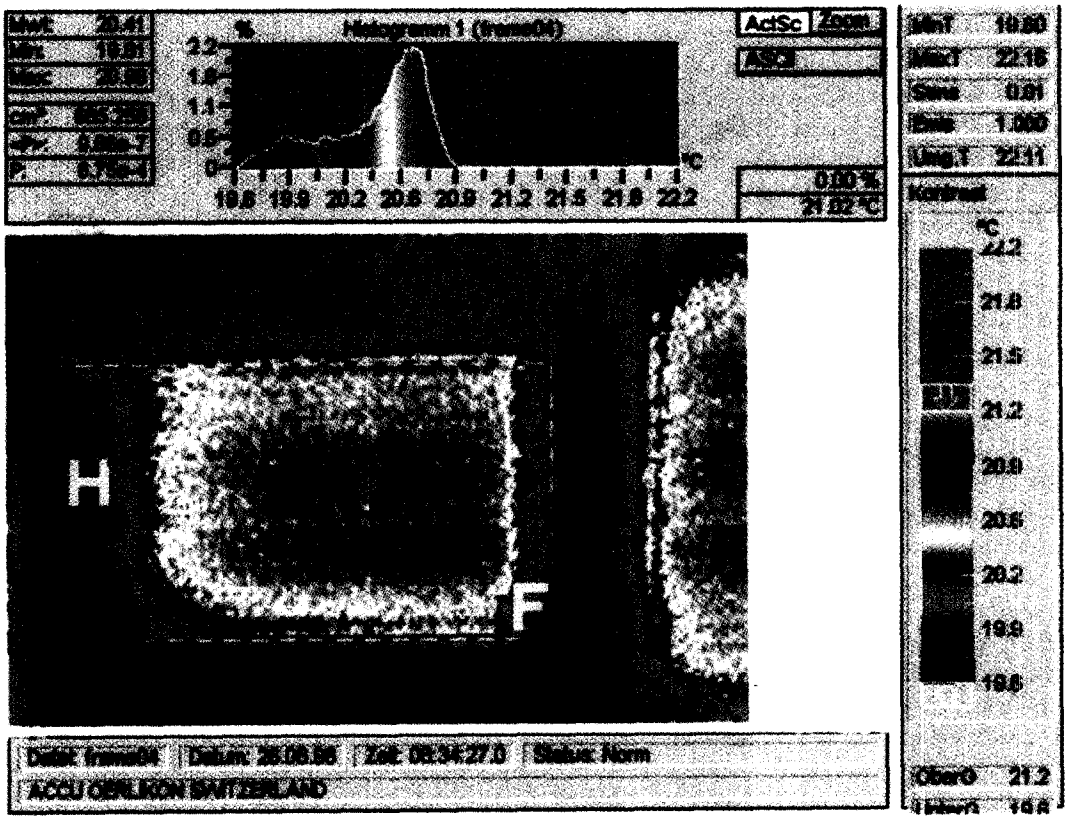

Fig. 10. False-colour temperature distribution image of a 2 V, 1000 Ah cell in a horizontal position (HPH) with (H) head space, (ST) plate stack and (F) foam bottom volume. Benign float condition of 2.25 V/cell at room temperature.

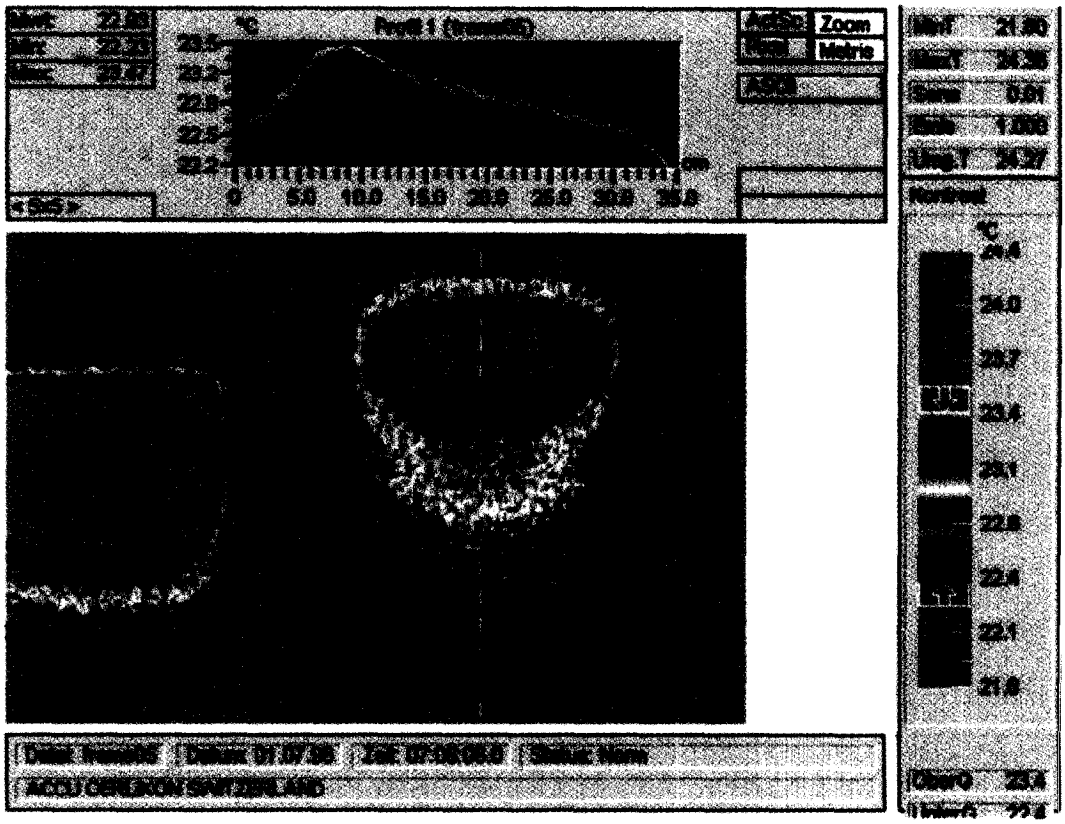

Fig. 11. False-colour temperature distribution image of a 2 V 1000 Ah cell in a vertical position (VP) under abusive float conditions of 2.50 V/cell. Note the concentration of heat production in the upper third of the plate stack.

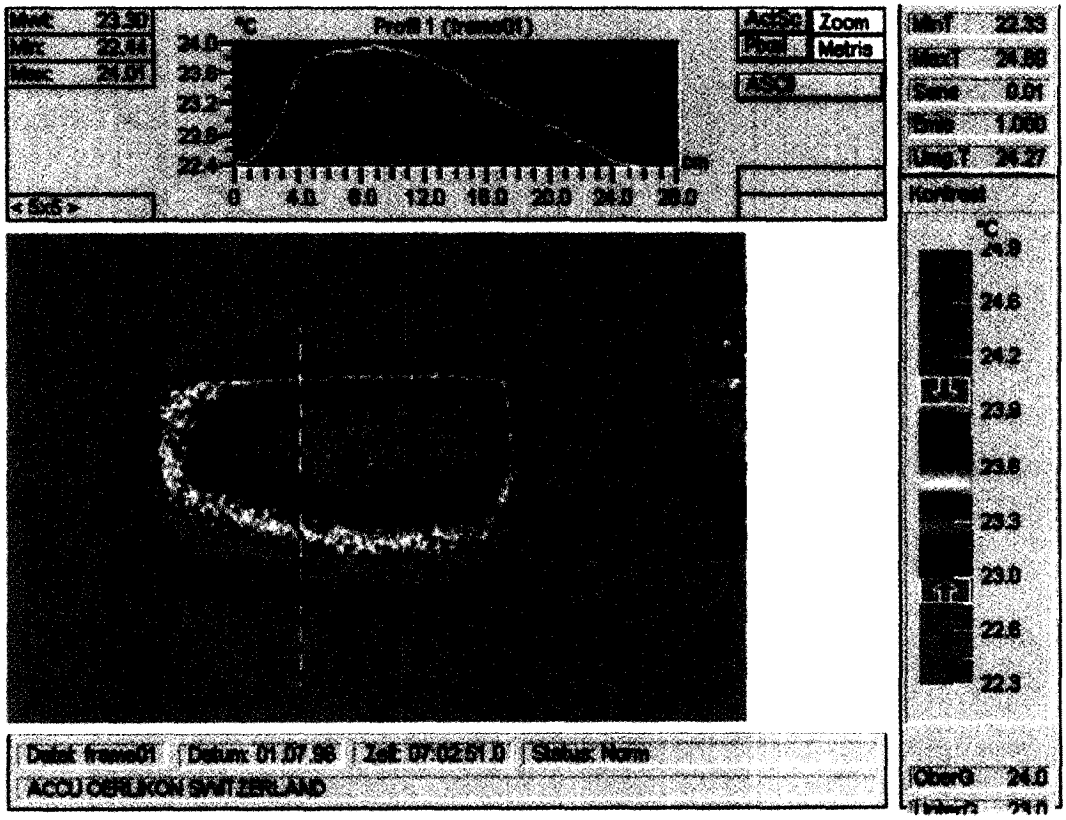

Fig. 12. False-colour temperature distribution image of a 2 V, 1000 Ah cell in a horizontal position (HPH) under abusive float conditions of 2.50 V/cell. Note the more extensive heat production area and its extension over the entire length of the stack.

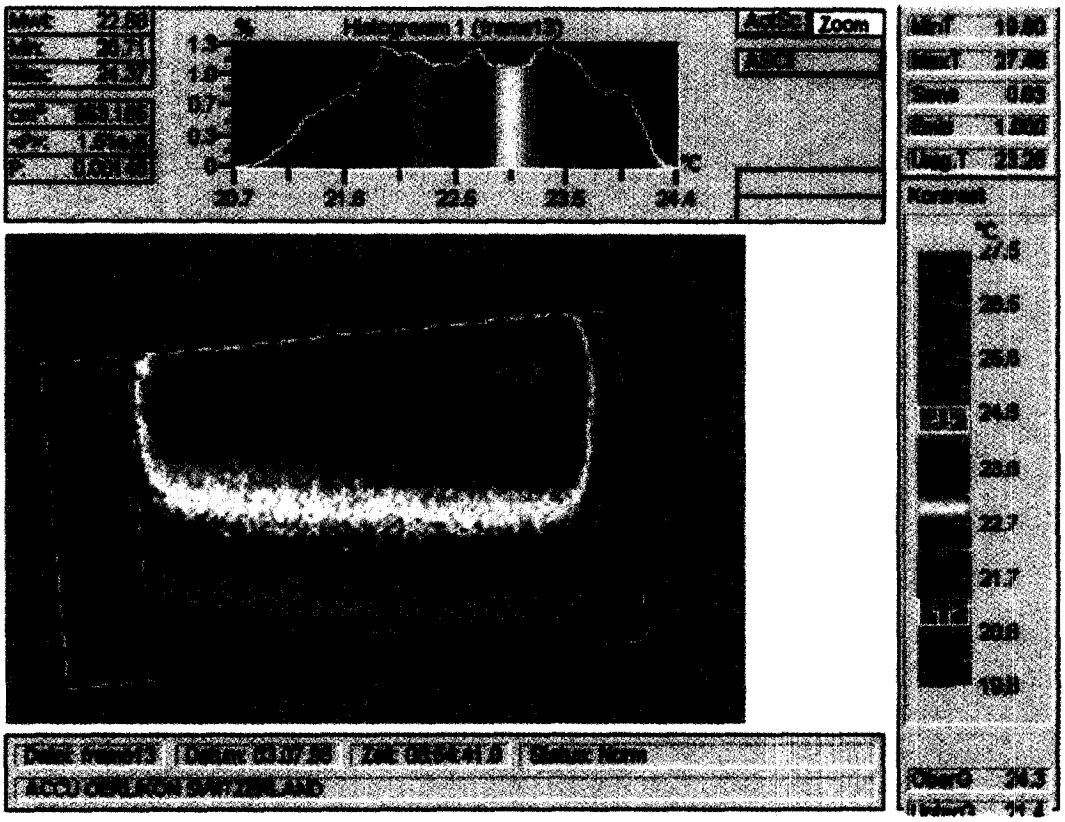

Fig. 13. False-colour temperature distribution image of a 2 V, 1000 Ah cell in a horizontal position (HPH) under abusive float conditions of 2.50 V/cell and tilted 5° forward. Note the heat production region migrates towards the end of the plate stack.

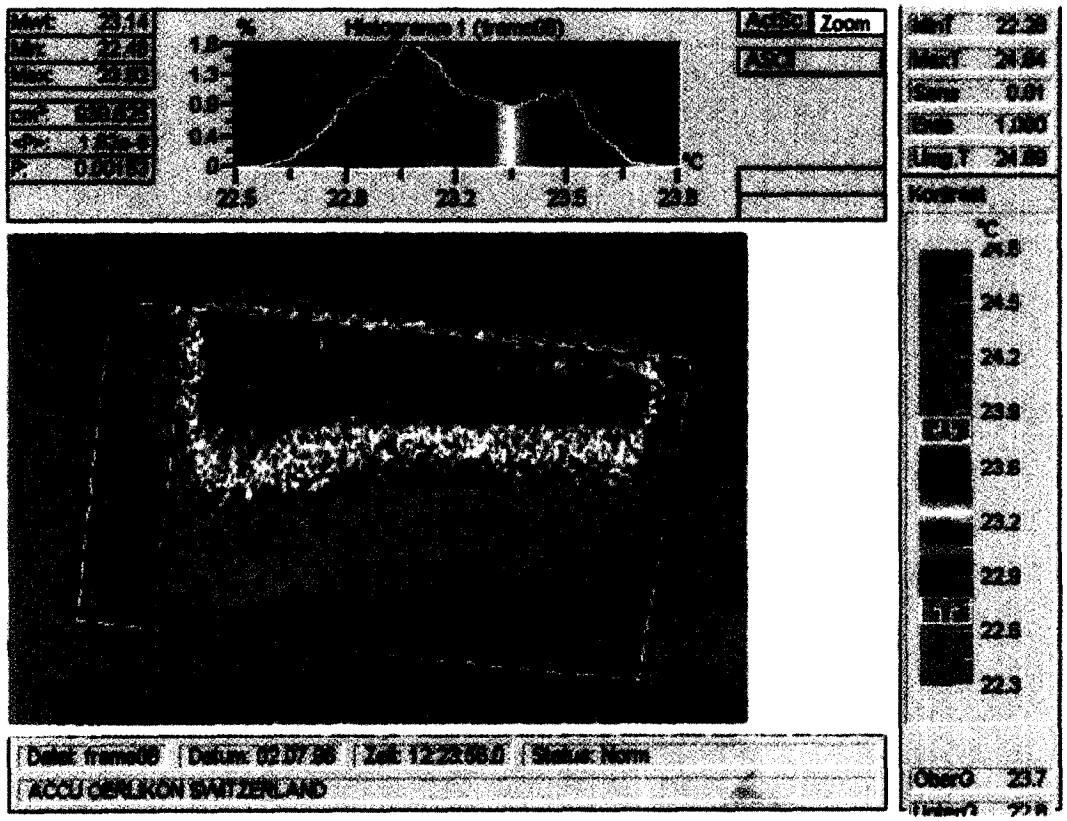

Fig. 14. False-colour temperature distribution image of a 2 V, 1000 Ah cell in a horizontal position (HPH) under abusive float conditions of 2.50 V/cell and tilted 5° backward. Note the heat production region migrates towards the front of the plate stack.

of a shorter current path and gravity induced, increased absorber porosity localizes the main current flow and the recombination reaction sites. The investigation of grid growth in cells operated under abusive conditions in this position revealed that the observed local horizontal growth values match quite well the observed temperature distribution image (i.e. 8.7% in the heat affected zone to 5.3% at plate bottom; 3.5% vertical grid growth).

For cells operated in the horizontal (HPH) position, the heat production region is slightly larger in volume and affects the entire length of the plate stack, see Fig. 12. Again, localized grid growth data reflect this temperature distribution (i.e. 11.0% in the heat-affected zone to 8.7% at plate bottom; 5.7% vertical grid growth).

From the two previously analysed temperature distribution cases, it was interesting to analyse eventual shifts in position of the heat production areas due to slight out-of-horizontal positioning of the plate stack. For this purpose, a 2 V, 1000 Ah cell was tilted 5° out of the horizontal and floated at 2.50 V/cell. Data presented in Figs. 13 and 14 show that the heat production volume followed, within 12 to 24 h, the change of the local electrolyte saturation levels in the absorber. With forward tilted cells, the heat production migrated to the back of the stack, and vice versa.

6. Conclusions

The use of thermal imaging of VRLA/AGM cells and monoblocs has proven to be a very valuable tool for detecting minute differences (0.05 °C) in internal temperature. The high transparency of ABS in the analysed IR wavelength, and the absence of blurring effects by liquid or gelled electrolyte, allow good spatial definition of the location and geometry of the heat source.

Heat imaging also allows the non-destructive determination of limiting cell(s) in VRLA batteries and, therefore, facilitates the detection and analysis of the limiting-cell component.

In large VRLA/AGM cells, local electrolyte saturation levels — induced by either gravity or deep cycling — can be easily detected by the related shift of the sites of the oxygen-recombination reaction within the cell stack.

References

[1] D. Berndt, *Varta Spezial Rep.*, No. 3, 1990.
[2] M. Kashimura, *Infrared Thermal Imaging System*, Nippon Avionics, Tokyo, Japan, 1993.